Journal of Photochemistry and Photobiology B: Biology
Volume 212, November 2020, 112044

UV-LED disinfection of Coronavirus: Wavelength effect

Yoram Gerchman [a], Hadas Mamane [b], Nehemya Friedman [c, d], Michal Mandelboim [c, d]

[a] Department of Biology and Environment, Faculty of Natural Science, University of Haifa and Oranim College, Tivon 3600600, Israel
[b] School of Mechanical Engineering, Faculty of Engineering, Tel Aviv University, Tel Aviv 69978, Israel
[c] Central Virology Laboratory, Ministry of Health, Chaim Sheba Medical Center, Tel-Hashomer, Ramat-Gan, Israel
[d] Department of Epidemiology and Preventive Medicine, School of Public Health, Tel-Aviv University, Israel

Received 28 July 2020, Revised 3 September 2020, Accepted 10 September 2020, Available online 28 September 2020.

https://doi.org/10.1016/j.jphotobiol.2020.112044

Highlights

- Corona virus HCoV-43 was found sensitive to UV-LED irradiation.

- Sensitivity was wavelength dependent with
  267 nm ~ 279 nm > 286 nm > 297 nm.
- Similar wavelength sensitivity was found for other viruses.
- UV-LEDs could probably be used in the fight against SARS-CoV-2 and COVID19.

Abstract

UV light-emitting diodes (UV LEDs) are an emerging technology and a UV source for pathogen inactivation, however low UV-LED wavelengths are costly and have low fluence rate. Our results suggest that the sensitivity of human Coronavirus (HCoV-OC43 used as SARS-CoV-2 surrogate) was wavelength dependent with
267 nm ~ 279 nm > 286 nm > 297 nm. Other viruses showed similar results, suggesting UV LED with peak emission at ~286 nm could serve as an effective tool in the fight against human Coronaviruses.

Graphical Abstract

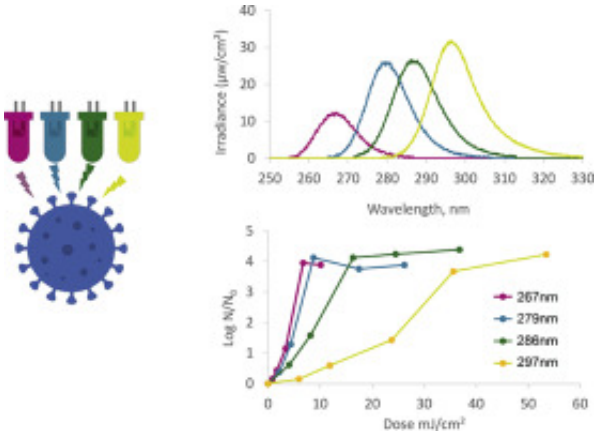

Download : Download high-res image (70KB) Download : Download full-size image

Previous Next

Keywords

UV-LEDs; Coronavirus; Corona; Wavelength; SARS; COVID19

1. Introduction

As the global prevalence of severe acute respiratory syndrome coronavirus 2 (SARS-CoV-2) outbreaks increases, there is a need to develop and demonstrate novel disinfection technologies for the inactivation of these viruses. SARS-CoV-2, the causal agent of COVID-19, is not only contagious through respiratory droplets, but can also spread through nasal, oral and eye mucus-contaminated surfaces [1]. Moreover, it has recently been suggested that SARS-CoV-2 could be airborne [2], although clear evidence for such transmission has not yet been presented. Furthermore, SARS-CoV-2's ability to survive in aerosols for at least 3 h and up to 72 h on plastic surfaces was recently demonstrated [3], suggesting long-term infection risks. Coronaviruses are 120–160 nm diameter, enveloped viruses with a single-stranded, non-segmented RNA genome, coated by a protein capsid and a lipid envelope. Damage to any of these components could result in inactivation of the virus [4].

UV irradiation is a common method for inactivation of pathogenic microorganisms, including viruses. Inactivation by UV could occur via several mechanisms, among them damage to nucleic acids [5,6], proteins [7], or internal production of oxygen radicals [8]. The mechanism of UV inactivation depends on the UV wavelength(s) used [7], and, atleast for some pathogens, UV sources with multiple emmision peaks (e.g. medium preassure lamps) were found to result in more effective inactivation, by activating multiple damage mechanisms [8]. UV inactivation was found as effective disinfection approach for many viruses, among them multiple bacteriophages (T4, T7, ϕ6, MS2, PR772 and ΦX174) [4,[9], [10], [11], [12], [13]], and many human and animal viruses, including SARS-CoV-1 [[14], [15], [16], [17], [18]].

UV light-emitting diodes (UV LEDs) are an emerging UV source for disinfection [19]. UV-LEDs allow for flexibility of design due to their small size and control of radiation patterns, have very short turn-on time, and require low voltage (and thus can be operated by a battery or a solar panel). UV LEDs have been found effective for disinfection of a variety of pathogens. However, UV LEDs have narrow emission spectra (Fig. 1), and lower wavelength UV LED tend to have a low output power (radiant flux; and are costly; on $/mW base) [19,20]. These restrictions make higher UV-LED wavelengths more attractive, but require testing the efficacy per pathogen. Numerous studies have examined the sensitivity of different microorganisms (including viruses) to UV LED at different wavelengths as

detailed in Table 1, for suspended viruses. However, no study to date has examined the efficiency of UV LEDs at different wavelengths on inactivation of the human Coronavirus. Here we have used the human Coronavirus OC43 (HCoV-OC43) as a surrogate to the SARS-CoV-2, to develop a dose-response curve for UV-LED at various wavelengths.

Download : Download high-res image (174KB) Download : Download full-size image

Fig. 1. Emission spectra of UV LEDs used in this study.

Table 1. Sensitivity of viruses to various UV wavelengths.

Virus type	Host	LED wave length (nm)	Virus enumeration method	Fluence (UV dose) (mJ/cm^2) for a given log reduction				Ref and comments
				1	2	3	4	
T7 Coliphage								
T7	*E. coli* ATCC 11303	255	PFU[a]	2.9	6.9	14	20	[27]
T7	*E. coli* ATCC 11303	275	PFU[a]	2.7	6	12	17	[27]
MS2 Coliphage								
MS2		255	PFU[a]	13	26	38		[28]
ATCC15597-B1	*E. coli* ATCC 15597	255	PFU[a]	25	50			[27]
ATCC15597-B1	*E. coli* ER2738	255	PFU[a]	19	42	72		[29]
ATCC15597-B1	*E. coli* Famp ATCC 700891	255	PFU[a]	12	28	45		[12]

MS2	*E. coli* Famp ATCC 700891	260	PFU[a]	13	28	44	58	[11]
ATCC15597-B1	*E. coli* Famp ATCC 700891	260	PFU[a]	12	30	43		[30]
ATCC15597-B1	*E. coli* ATCC 15597 C3000	260	PFU[a]	15	32	48		[31] Flow reactor
ATCC15597-B1	*E. coli* Famp ATCC 700891	265	PFU[a]	15	32	51		[12]
ATCC15597-B1		265	PFU[a]	18.1	47.1	76.1	105.2	[32]
ATCC15597-B1	*E. coli* ATCC 15597	275	PFU[a]	25	55			[27]
ATCC15597-B1	*E. coli* Famp ATCC 700891	280	PFU[a]	18	39	60		[30]
ATCC15597-B1		280	PFU[a]	30.3	60.9	91.5	122.1	[32]
ATCC15597-B1	*E. coli* K12 A/ λ(F+)	285	PFU[a]	35	70	106		[33]
ATCC15597-B1	*E. coli* Famp ATCC 700891	285	PFU[a]	25	52	95		[12]
ATCC15597-B1		300		412.8	763.4	1114.1	1464.7	[32]
Phi X 174								
φX174		255	PFU[a]	1.7	3.3	5.1		[28]
φX174		280	PFU[a]	2.8	5.1	8.6		[28]
Qβ								
Qβ		255	PFU[a]	13	23			[28]
Qβ	*E. coli* ATCC 15597 C3000	260	PFU[a]	9	19	29	41	[31] Flow reactor

ATCC23631-B1	E. coli K-12 A/ λ (F+)	265	PFU[a]	8.9	19.9	31.0	42.0	[32]
Qβ		280	PFU[a]	28				[28]
ATCC23631-B1	E. coli K-12 A/ λ (F+)	280	PFU[a]	16.0	35.1	54.1	73.2	[32]
ATCC23631-B1	*E. coli* K12 A// λ (F+)	285	PFU[a]	27	54	81		[33]
ATCC23631-B1	E. coli K-12 A/ λ (F+)	300	PFU[a]	100.0	304.8	509.7	714.5	[32]
Enterovirus								
Coxsackievirus A10 (CVA10, Kowalik strain		260	ICC-RTqPCR	5	8		15	[34]
Polivirus 1 (PV1, Mahoney strain)		260	ICC-RTqPCR		8			[34]
Enterovirus 70 EV70 ()J670/71 strain)		260	ICC-RTqPCR		10			[34]
Echovirus 30 (Echo30, Bastianni strain)		260	ICC-RTqPCR		13			[34]
Coxsackievirus A10(CVA10, Kowalik strain		280	ICC-RTqPCR		12	15		[34]
Polivirus 1 (PV1, Mahoney strain)		280	ICC-RTqPCR		11			[34]
Enterovirus 70 (EV70, J670/71 strain)		280	ICC-RTqPCR		12			[34]
Echovirus 30 (Echo30, Bastianni		280	ICC-RTqPCR		15			[34]

strain)								
Adenovirus								
Adenovirus 2 – HadV2-ATCCvr-846 Manassas, VA	A549 human lung carcinoma cells-ATCC-CCL-185	260	TCVA[b] and ICC-qPCR[c]	40	69	87	110	[30]
Adenovirus 2 – HadV2-ATCCvr-846 Manassas, VA	A549 human lung carcinoma cells-ATCC-CCL-185	280	TCVA[b] and ICC-qPCR[c]	48	74	95	115	[30]
Adenovirus Type 5 ATCC VR5	A549 cell line (CCL-185)	285	PFA[d]	44	82	126		[33]
Vesivirus								
Feline calicivirus ATCC-VR-782	Crandell Rees feline kidney cells (CRFK, ATCC CCL-94)	265	N/A	6.7	15.6	24.5	33.4	[32]
Feline calicivirus ATCC-VR-782	Crandell Rees feline kidney cells (CRFK, ATCC CCL-94)	280	N/A	9.0	18.9	28.9	38.8	[32]
Feline calicivirus ATCC-VR-782	Crandell Rees feline kidney cells (CRFK, ATCC CCL-94)	300	N/A	139.1	286.8	434.6	582.3	[32]

Influenza virus								
H1N1 subtype. Viral suspensions of H1N1 subtype (strain A/Puerto Rico/8/1934)	Madin-Darby canine kidney (MDCK) cells	280	ICC-RTqPCR[c]; PFA[d]; FFA[e]	20	33	50	125	[35]
H1N1 subtype. Viral suspensions of H1N1 subtype (strain A/Puerto Rico/8/1934)	Madin-Darby canine kidney cells (MDCK)	310	ICC-RTqPCR[c]; PFA[d]; FFA[e]	250	430	1150		[35]
H1N1 subtype. Viral suspensions of H1N1 subtype (strain A/Puerto Rico/8/1934)	Madin-Darby canine kidney cells (MDCK)	365	ICC-RTqPCR[c]; PFA[d]; FFA[e]	7000	42,000			[35]
Coronavirus								
SARS-CoV-2	Vero cells	280 ± 5	PFA[d]	3.75		37.5		[36]
HCoV-OC43	Vero-E6 cells	267	ICC-RTqPCR	3.4	5.0	5.7	6.8	Current study
HCoV-OC43	Vero-E6 cells	279	ICC-RTqPCR	3.5	5.5	7.0	8.7	Current study
HCoV-OC43	Vero-E6 cells	286	ICC-RTqPCR	5.8	9.5	12.9	16.4	Current study
HCoV-OC43	Vero-E6 cells	297	ICC-RTqPCR	17.5	26.8	32.0	47.0	Current study

a

PFU: Plaques Forming Units. Bacteriophages are mixed with the bacteria in melted soft agar media and poured on agar media (top layer). Plaques of dead bacteria appear as hallows in the bacteria turbidity.

b

TCVA: Total Culturable Virus Assay. Briefly, the virus is serially diluted and added to a culture of host cells. Most Probable Number is calculated by host cell lysis as evidence for viable virus presence.

c

ICC-(RT)qPCR: Integrated Cell Culture (RealTime) Quantitative PCR. Briefly, viruses are diluted and incubated with host cells. After incubation, cells are washed to remove extracellular viruses, broken to release viruses, and virus genome copy number is analyzed by quantitative polymerase chain reaction (qPCR). For RNA viruses a reverse transcriptase (RT) reaction to convert RNA to DNA precede the qPCR (hence ICC-RTqPCR).

d

PFA: Plaque-Forming Assay. Similar to PFU ([a]) but after infection and incubation host cells are fixed, stained, and plaques identified and counted.

e

FFA: Focus-Forming Assay. Briefly, after infection and incubation host cells are fixed labeled with antibody against viral proteins and the antibody fluorescently labeled. Infected cells are counted by fluorescence microscopy.

2. Materials and Methods

2.1. UV-LED Irradiation Systems

UV-exposure experiments were conducted using a UV-LED system (PearlBeam) from AquiSense Technologies (Charlotte, NC, USA) with selected LEDs. The first, “circular system”,included LEDs with peak emission wavelengths at 279 nm and 297 nm (model PearlLab Beam™) with an overall circular area of 43.8 cm^2 (Fig. 2); the second system a “rectangular system” was custom-made and included LEDs with nominated peak emission at 267 nm and 286 nm wavelengths, designed in collaboration with AquiSense with an overall area of 15.7 cm × 11.5 cm, covering multiple multitier plate (Fig. 2) [21].

Download : Download high-res image (693KB) Download : Download full-size image

Fig. 2. Schematic layout of the inactivation experiment with the 24-well plate used in this study. Numbers in wells represent the incident irradiance (mW/cm^2) as measured for each particular well location (Top-left, 267 nm; top-right, 279 nm; bottom-left, 286 nm; bottom-

right, 297 nn). The red encircle irradiation area for one time/dose irradiation point (left: 4-well column, for 267/286 nm rectangular system; right: 2 × 2 wells for 279/297 nm round system). (For interpretation of the references to colour in this figure legend, the reader is referred to the web version of this article.)

The UV spectra of the UV-LED wavelengths used in this study were measured using an Ocean Optics USB4000 spectroradiometer equipped with a cosine corrector. The 267 nm and 286 nm UV LEDs exhibited peak wavelength emissions at 267.2 nm (hereafter 267) and 285.8 nm (hereafter 286), respectively, with full width at half maximum (FWHM) bandwidths of 12.3 nm and 13.5 nm, respectively. The 279 nm and 297 nm UV LEDs exhibited peak wavelength emissions at 278.8 nm (hereafter 279) and 296.6 nm (hereafter 297) respectively, with FWHM bandwidths of 20 nm and 15 nm, respectively. Fig. 1 shows the emission spectra of each UV LED used in this study, measured at the approximate center of the exposure area.

2.2. Virus Irradiation

Virus HCoV-OC43 was used in all experiments. The virus was propagated as previously described [22] and diluted just before irradiation in PBS to 8×10^5 PFU/ml. For each irradiation experiment 50 μl of virus suspension (equivalent to 4000 PFU; measured by PFA, see Table 1 note 'd') was placed in each well of a black 24-well plate, and all well were covered with black insulation tape. Before each irradiation experiment, the tape was removed from four wells (column for the "rectangular system", or 2 × 2 for the "round system"; Fig. 2), and the plate exposed to the designated irradiation wavelength and time. After each irradiation, the irradiated wells were covered again, and the next four wells exposed and irradiated, until all wells had been irradiated (except for the zero-irradiation control), all similar to described in [21]. Because inactivation occurred only within the exposed four wells, and the well wall material was black, the irradiance delivered to each well was independent of that to the neighboring wells.

UV optical absorbance of the virus suspension was measured at 220–400 nm range using Nanodrop spectrophotometer, and transmittance (%UVT) was calculated as %T = antilog(2-absorbance). %UVT was found to be higher than 98% throughout all wavelength range. Log inactivation was calculated as log (N_0/N), where N_0 and N are virus concentration before and after irradiation, respectively.

2.3. Irradiation Dose

Incident irradiance (fluence) was measured for each well separately using Ocean Optics USB4000 spectroradiometer with fiber core diameter of 600 μm (QP600-2-VIS-NIR), the small footprint of the fiber optic end allowing accurate measurements. A printout of the 24-well plate was placed under the UV LED system and the spectroradiometer optic fiber end was placed on the geometric center of the measured well on the printout, perpendicular to the surface and facing the UV LEDs [2]. Height was adjusted to confirm that the fiber end was in the same distance from the UV LED as was the plate bottom in the irradiation experiments. Fig. 2 shows the incident irradiance measured. For each LED, measurements for all wells in the plate were averaged to obtain average incident irradiances, resulting in (all in mW/cm^2): $LED_{267} = 0.16 \pm 0.01$, $LED_{279} = 0.43 \pm 0.01$, $LED_{286} = 0.39 \pm 0.02$, $LED_{297} = 0.58 \pm 0.02$. As evident from Fig. 2, the variation in the incident irradiance values among wells exposed in each experiment was less than 5% of the average between those wells (either column or square), and thus negligible. Given this, irradiation dose was calculated by simply multiplying the fluence (mW/cm^2) by exposure time (seconds; up to 60 s for 267 and 279 nm and up to 90 s for 286 and 297 nm).

2.4. Virus Quantification by RT-qPCR (ICC-RTqPCR)

After irradiation, 50 μl Eagle's Minimum Essential Medium supplemented with 2% (v/v) fetal calf serum was added to each well; the content was mixed by pipetation, and 50 μl was transferred to a 96-well plate (Applied Biosystems) containing 24-h-old and 80–90% confluent Vero-E6 cells in the same medium, resulting in a multiplicity of infection for the virus of 0.1 (i.e. up to 2000 PFU/well; allowing quantification of 3-log reduction). Cells and viruses were grown in a humidified incubator with 5% CO_2 at 33 °C for 72 h, after which total RNA was extracted from the above cells using a MagNA Pure 96 Instrument (Roche Life Science) according to the manufacturer's protocol. Viral load was determined by RT-qPCR (using Applied Biosystems 7500 Real-Time PCR System) as described by Dare et al. (2007) [23] and compared against a calibration curve constructed from virus suspensions of known titers.

3. Results and Discussion

3.1. Inactivation by UV Irradiation

The dose (fluence) response curve of HCoV-OC43 to UV LEDs with different peak wavelengths is presented in Fig. 3. The UV LEDs at 267 and 279 nm were very effective at inactivating the Coronavirus (3-log inactivation at irradiation 6–7 mJ/cm^2), whereas longer UV-LED wavelengths (i.e., 286 and 297 nm) required higher doses for 3-log inactivation (13 mJ/cm^2 and 32 mJ/cm^2, respectively), nevertheless, even these wavelengths resulted in

effective inactivation. Interestingly, none of the wavelength tested showed a tailing effect (characterized by a decrease in the slope of the inactivation curve) as demonstrated in other studies [[24], [25], [26]]. The reason for the high standard deviation at the higher dose/lower survival zones of the curves is an artifact due to lack of precision in enumerating the low number of survivors, thus limit of quantification (LOQ) of the assay was determined as reduction of 3 $\log_{10}$ PFU/mL. Attempt to increase the initial virus concentration resulted in aggregation as was evident by high variation in the N_0 counts (data not shown).

Fig. 3. Dose (fluence) response curve of the HCoV-OC43 to UV-LEDs. N is virus count after the designated irradiation and N_0 at time zero (without irradiation).

The sensitivity of various viruses to different UV wavelengths is presented in Table 1 and compared to the sensitivity of HCoV-OC43 tested here. Generally, the wavelength ~ 260 nm showed slightly higher effectivity then ~280 nm, with (from high to low sensitivity) PHI X 174 ≅ HCoV-OC43 > T7 > Vesivirus > Enterovirus > SARS-CoV-2 > Influenza ≅ Qβ> MS2 > Adenovirus (according to the 2- and 3-log inactivation data of Table 1; compared for similar wavelengths). Increasing the wavelength to ~300 nm resulted in dramatic drop in disinfection effectivity (e.g. for MS2, Qβ, feline calicivirus and H1N1) with ~10-fold higher dose needed as compared to 280–290 nm. In the same manner, the HCoV-OC43 in this study showed similar dose-response to irradiation at 267 and 279 nm, somewhat lower sensitivity to 286 nm, and a sharp increase in the required dose when irradiated at 297 nm (Fig. 3). The data presented in Fig. 3 and in Table 1 demonstrate that indeed UV-LED with peak emission at ~286 nm (but not much higher) could offer efficient inactivation of many viruses, including the corona virus family, thus overcoming the current limitations of the lower UV-LED wavelengths.

3.2. The Human Coronavirus OC43 (HCoV-OC43) as a Surrogate for SARS-CoV-2

The Coronaviridae are the largest enveloped RNA viruses, having a positive single-stranded RNA molecule that ranges between 26.2 and 31.7 kb [[37], [38], [39]]. Both HCoV-OC43 and SARS-CoV-2 belong to the *Betacoronavirus* genus, dividing to *Embecovirus* and *Sarbecovirus* subgenus respectively [40,41]. HCoV-OC43 and SARS-CoV-2 genomes size are alike, ~30,600 bp (e.g. GI numbers 530,802,586, 530,802,542) vs 29,903 bp respectively (Wuhan-Hu-

1 complete reference genome NC_045512.2). All CoVs encodes 4 essential structural proteins, spike (S), envelope (E), membrane (M) and nucleocapsid (N) [42]. These viruses share structural similarities, with several differences that could affect viral proteins interactions and functions [41]. For example, the M protein is the most abundant structural protein of coronaviruses, interacts with other viral proteins and is critical for viral assembly and may contribute to viral pathogenesis [41,43]. The M protein is modified by O-linked glycosylation in the N-terminal domain in HCoV-OC43 or by N-linked glycosylation at most other coronaviruses. Both glycosylation types are not required for virion assembly, however O-linked glycosylation is associated with induction of type I interferon [43]. HCoV-OC43 possess ns12.9 accessory protein, analogous to the SARS-CoV 3a protein, a viroporin that regulates virus production [44,45]. Both HCoV-OC43 and SARS-CoV-2 uses S protein to attach the host membrane, however HCoV-OC43 employ glycan-based receptors with 9-*O*-acetylated sialic acid and SARS-CoV-2 use the cell surface peptidase ACE2 [41]. Furthermore, Embecoviruses express a unique hemagglutinin-esterase (HE) transmembrane protein that may facilitate virion attachment via its sialic acid-binding activity and could mediated release of progeny virions by its esterase activity [37,41]. HCoV-OC43 had serological cross-reactivity with SARS-CoV N protein [46] but not to sera of SARS-CoV-2-positive patients [47]. To conclude, both human Coronaviruses HCoV-OC43 and SARS-CoV-2 are very similar, thus it is reasonable to suggest a human Coronavirus HCoV-OC43 as a surrogate for SARS-CoV-2, and our future work will confirm these results by testing the impact of LEDs and their combinations on SARS-CoV-2.

Declaration of Competing Interest

The authors declare that they have no known competing financial interests or personal relationships that could have appeared to influence the work reported in this paper.

Acknowledgements

This work was supported by the MAGNETON Program of the Israel Innovation Authority [Grant no. 67827].

Recommended articles Citing articles (0)

References

[1] WHO
Transmission of SARS-CoV-2: Implications for Infection Prevention Precautions

https://www.who.int/news-room/commentaries/detail/transmission-of-sars-cov-2-implications-for-infection-prevention-precautions (2020)
Google Scholar

[2] E. Nardell, P. Lederer, H. Mishra, R. Nathavitharana, G. Theron
Cool but dangerous: how climate change is increasing the risk of airborne infections
Indoor Air, 30 (2) (2020), pp. 195-197
CrossRef View Record in Scopus Google Scholar

[3] N. Van Doremalen, T. Bushmaker, D.H. Morris, M.G. Holbrook, A. Gamble, B.N. Williamson, A. Tamin, J.L. Harcourt, N.J. Thornburg, S.I. Gerber, J.O. Lloyd-Smith
Aerosol and surface stability of SARS-CoV-2 as compared with SARS-CoV-1
N. Engl. J. Med., 382 (2020), pp. 1564-1567
CrossRef View Record in Scopus Google Scholar

[4] A.I. Silverman, A.B. Boehm
Systematic review and meta-analysis of the persistence and disinfection of human coronaviruses and their viral surrogates in water and wastewater
Environ. Sci. Technol. Lett. (2020), 10.1021/acs.estlett.0c00313
Google Scholar

[5] R.P. Rastogi, A. Kumar, M.B. Tyagi, R.P. Sinha
Molecular mechanisms of ultraviolet radiation-induced DNA damage and repair
J. Nucleic Acids (2010)
0.4061/2010/592980
Google Scholar

[6] S.E. Beck, R.A. Rodriguez, M.A. Hawkins, T.M. Hargy, T.C. Larason, K.G. Linden
Comparison of UV-induced inactivation and RNA damage in MS2 phage across the germicidal UV spectrum
Appl. Environ. Microbiol., 82 (5) (2016), pp. 1468-1474
View Record in Scopus Google Scholar

[7] A.C. Eischeid, K.G. Linden
Molecular indications of protein damage in adenoviruses after UV disinfection
Appl. Environ. Microbiol., 77 (3) (2011), pp. 1145-1147
View Record in Scopus Google Scholar

[8] Y. Gerchman, V. Cohen-Yaniv, Y. Betzalel, S. Yagur-Kroll, S. Belkin, H. Mamane
The involvement of superoxide radicals in medium pressure UV derived

inactivation
Water Res., 161 (2019), pp. 119-125
Article Download PDF View Record in Scopus Google Scholar

[9] H. Mamane, H. Shemer, K.G. Linden
Inactivation of *E. coli*, *B. subtilis* spores, and MS2, T4, and T7 phage using UV/H2O2 advanced oxidation
J. Hazard. Mater., 146 (3) (2007), pp. 479-486
Article Download PDF View Record in Scopus Google Scholar

[10] D.B. Misstear, L.W. Gill
The inactivation of phages MS2, Φx174 and PR772 using UV and solar photocatalysis
J. Photochem. Photobiol. B, 107 (1) (2012), pp. 1-8
Article Download PDF View Record in Scopus Google Scholar

[11] K.A. Sholtes, K. Lowe, G.W. Walters, M.D. Sobsey, K.G. Linden, L.M. Casanova
Comparison of ultraviolet light-emitting diodes and low-pressure mercury-arc lamps for disinfection of water
Environ. Technol., 37 (17) (2016), pp. 2183-2188
CrossRef View Record in Scopus Google Scholar

[12] N.M. Hull, K.G. Linden
Synergy of MS2 disinfection by sequential exposure to tailored UV wavelengths
Water Res., 143 (2018), pp. 292-300
Article Download PDF View Record in Scopus Google Scholar

[13] Y. Ye, P.H. Chang, J. Hartert, K.R. Wigginton
Reactivity of enveloped virus genome, proteins, and lipids with free chlorine and UV254
Environ. Sci. Technol., 52 (14) (2018), pp. 7698-7708
CrossRef View Record in Scopus Google Scholar

[14] H. Kariwa, N. Fujii, I. Takashima
Inactivation of SARS coronavirus by means of povidone-iodine, physical conditions and chemical reagents
Dermatology, 212 (2006), pp. 119-123
Suppl. 1
CrossRef View Record in Scopus Google Scholar

[15] M.E. Darnell, K. Subbarao, S.M. Feinstone, D.R. Taylor
Inactivation of the coronavirus that induces severe acute respiratory syndrome, SARS-CoV
J. Virol. Methods, 121 (1) (2004), pp. 85-91
Article Download PDF View Record in Scopus Google Scholar

[16] B. Pendyala, A. Patras, D. D'Souza
Genomic modeling as an approach to identify surrogates for use in experimental validation of SARS-CoV-2 and HuNoVs inactivation by UV-C treatment
bioRxiv (2020), 10.1101/2020.06.14.151290
http://biorxiv.org/content/early/2020/06/16/2020.06.14.151290.abstract
Google Scholar

[17] E.R. Blatchley III, B. Petri, W. Sunc
SARS-CoV-2 UV Dose-Response Behavior
International Ultraviolet Association (IUVA) White Paper (2020)
https://iuva.org/resources/covid-19/SARS%20CoV2%20Dose%20Response%20White%20Paper.pdf
Google Scholar

[18] S.M. Duan, X.S. Zhao, R.F. Wen, J.J. Huang, G.H. Pi, S.X. Zhang, J. Han, S.L. Bi, L. Ruan, X.P. Dong
Stability of SARS coronavirus in human specimens and environment and its sensitivity to heating and UV irradiation
Biomed. Environ. Sci., 16 (3) (2003), pp. 246-255
View Record in Scopus Google Scholar

[19] J. Chen, S. Loeb, J.H. Kim
LED revolution: fundamentals and prospects for UV disinfection applications
Environ. Sci. Water Res. Technol., 3 (2) (2017), pp. 188-202
View Record in Scopus Google Scholar

[20] O. Lawal, J. Cosman, J. Pagan
UV-C LED devices and systems: current and future state
IUVA News, 20 (1) (2018), pp. 22-28
https://iuvanews.com/stories/pdf/IUVA_2018_Quarter1_Lawal-article_hyperlinks.pdf
View Record in Scopus Google Scholar

[21] Y. Betzalel, Y. Gerchman, V. Cohen-Yaniv, H. Mamane
Multiwell plates for obtaining a rapid microbial dose-response curve in UV- LED

systems
J. Photochem. Photobiol. B, 207 (2020), p. 111865
Article Download PDF Google Scholar

[22] D.E. Kim, J.S. Min, M.S. Jang, J.Y. Lee, Y.S. Shin, C.M. Park, J.H. Song, H.R. Kim, S. Kim, Y.H. Jin, S. Kwon
Natural bis-benzylisoquinoline alkaloids-tetrandrine, fangchinoline, and cepharanthine, inhibit human coronavirus OC43 infection of MRC-5 human lung cells
Biomolecules, 9 (11) (2019), p. 696
CrossRef View Record in Scopus Google Scholar

[23] R.K. Dare, A.M. Fry, M. Chittaganpitch, P. Sawanpanyalert, S.J. Olsen, D.D. Erdman
Human coronavirus infections in rural Thailand: a comprehensive study using real-time reverse-transcription polymerase chain reaction assays
J. Infect. Dis., 196 (9) (2007), pp. 1321-1328
CrossRef View Record in Scopus Google Scholar

[24] G.J. Galasso, D.G. Sharp
Effect of particle aggregation on the survival of irradiated vaccinia virus
J. Bacteriol., 90 (4) (1965), pp. 1138-1142
CrossRef View Record in Scopus Google Scholar

[25] Q.S. Meng, C.P. Gerba
Comparative inactivation of enteric adenoviruses, poliovirus and coliphages by ultraviolet irradiation
Water Res., 30 (11) (1996), pp. 2665-2668
Article Download PDF View Record in Scopus Google Scholar

[26] M.J. Mattle, T. Kohn
Inactivation and tailing during UV254 disinfection of viruses: contributions of viral aggregation, light shielding within viral aggregates, and recombination
Environ. Sci. Technol., 46 (18) (2012), pp. 10022-10030
View Record in Scopus Google Scholar

[27] C. Bowker, A. Sain, M. Shatalov, J. Ducoste
Microbial UV fluence-response assessment using a novel UV-LED collimated beam system
Water Res., 45 (5) (2011), pp. 2011-2019
Article Download PDF View Record in Scopus Google Scholar

[28] Y. Aoyagi, M. Takeuchi, K. Yoshida, M. Kurouchi, N. Yasui, N. Kamiko, T. Araki, Y. Nanishi
Inactivation of bacterial viruses in water using deep ultraviolet semiconductor light-emitting diode
J. Environ. Eng., 137 (12) (2011), pp. 1215-1218
View Record in Scopus Google Scholar

[29] R. Simons, U.E. Gabbai, M.A. Moram
Optical fluence modelling for ultraviolet light emitting diode-based water treatment systems
Water Res., 66 (2014), pp. 338-349
Article Download PDF View Record in Scopus Google Scholar

[30] S.E. Beck, H. Ryu, L.A. Boczek, J.L. Cashdollar, K.M. Jeanis, J.S. Rosenblum, O.R. Lawal, K.G. Linden
Evaluating UV-C LED disinfection performance and investigating potential dual-wavelength synergy
Water Res., 109 (2017), pp. 207-216
Article Download PDF View Record in Scopus Google Scholar

[31] R.M. Jenny, O.D. Simmons III, M. Shatalov, J.J. Ducoste
Modeling a continuous flow ultraviolet Light Emitting Diode reactor using computational fluid dynamics
Chem. Eng. Sci., 116 (2014), pp. 524-535
Article Download PDF View Record in Scopus Google Scholar

[32] K. Oguma, S. Rattanakul, M. Masaike
Inactivation of health-related microorganisms in water using UV light-emitting diodes
Water Sci. Technol. Water Supply, 19 (5) (2019), pp. 1507-1514
CrossRef View Record in Scopus Google Scholar

[33] K. Oguma, S. Rattanakul, J.R. Bolton
Application of UV light-emitting diodes to adenovirus in water
J. Environ. Eng., 142 (3) (2016), Article 04015082
CrossRef Google Scholar

[34] H. Woo, S.E. Beck, L.A. Boczek, K.M. Carlson, N.E. Brinkman, K.G. Linden, O.R. Lawal, S.L. Hayes, H. Ryu
Efficacy of inactivation of human enteroviruses by dual-wavelength germicidal

ultraviolet (UV-C) light emitting diodes (LEDs)
Water, 11 (6) (2019), p. 1131
CrossRef Google Scholar

[35] R. Nishisaka-Nonaka, K. Mawatari, T. Yamamoto, M. Kojima, T. Shimohata, T. Uebanso, M. Nakahashi, T. Emoto, M. Akutagawa, Y. Kinoucha, T. Wada
Irradiation by ultraviolet light-emitting diodes inactivates influenza a viruses by inhibiting replication and transcription of viral RNA in host cells
J. Photochem. Photobiol. B, 189 (2018), pp. 193-200
Article Download PDF View Record in Scopus Google Scholar

[36] H. Inagaki, A. Saito, H. Sugiyama, T. Okabayashi, S. Fujimoto
Rapid inactivation of SARS-CoV-2 with deep-UV LED irradiation
Emerg. Microbes Infect., 9 (1) (2020), pp. 1744-1747, 10.1080/22221751.2020.1796529
CrossRef Google Scholar

[37] P.C. Woo, Y. Huang, S.K. Lau, K.Y. Yuen
Coronavirus genomics and bioinformatics analysis
Viruses, 2 (8) (2010), pp. 1804-1820, 10.3390/v2081803
CrossRef View Record in Scopus Google Scholar

[38] M.M.C. Lai, S. Perlman, L.J. Anderson
D.M. Knipe, P.M. Howley (Eds.), Coronaviridae, Fields virology (5th ed), Lippincott Williams & Wilkins, Philadelphia, PA (2007), pp. 1305-1335
View Record in Scopus Google Scholar

[39] R. McBride, M. Van Zyl, B.C. Fielding
The coronavirus nucleocapsid is a multifunctional protein
Viruses, 6 (8) (2014), pp. 2991-3018, 10.3390/v6082991
CrossRef View Record in Scopus Google Scholar

[40] A. Wartecki, P. Rzymski
On the coronaviruses and their associations with the aquatic environment and wastewater
Water, 12 (6) (2020), p. 1598, 10.3390/w12061598
CrossRef Google Scholar

[41] D.X. Liu, J.Q. Liang, T.S. Fung
Human Coronavirus-229E, -OC43, -NL63, and -HKU1, Reference Module in Life Sciences

(2020), 10.1016/B978-0-12-809633-8.21501-X
B978-0-12-809633-8.21501-X. (Epub 2020 May 7. PMCID: PMC7204879)
Google Scholar

[42] Y. Chen, Q. Liu, D. Guo
Emerging coronaviruses: genome structure, replication, and pathogenesis
J. Med. Virol., 92 (4) (2020), pp. 418-423, 10.1002/jmv.25681
CrossRef View Record in Scopus Google Scholar

[43] T.S. Fung, D.X. Liu
Post-translational modifications of coronavirus proteins: roles and function
Future Virol., 13 (6) (2018), pp. 405-430, 10.2217/fvl-2018-0008
(PMID: 32201497; PMCID: PMC7080180)
CrossRef View Record in Scopus Google Scholar

[44] R. Zhang, K. Wang, X. Ping, W. Yu, Z. Qian, S. Xiong, B. Sun
The ns12.9 accessory protein of human coronavirus OC43 is a viroporin involved in virion morphogenesis and pathogenesis
J Virol., 89 (22) (2015), pp. 11383-11395, 10.1128/JVI.01986-15
(PMID: 26339053; PMCID: PMC4645656)
View Record in Scopus Google Scholar

[45] R. Zhang, K. Wang, W. Lv, W. Yu, S. Xie, K. Xu, W. Schwarz, S. Xiong, B. Sun
The ORF4a protein of human coronavirus 229E functions as a viroporin that regulates viral production
Biochim. Biophys. Acta, 1838 (4) (2014), pp. 1088-1095, 10.1016/j.bbamem.2013.07.025
Article Download PDF View Record in Scopus Google Scholar

[46] D.M. Patrick, M. Petric, D.M. Skowronski, R. Guasparini, T.F. Booth, M. Krajden, P. McGeer, N. Bastien, L. Gustafson, J. Dubord, D. Macdonald, S.T. David, L.F. Srour, R. Parker, A. Andonov, J. Isaac-Renton, N. Loewen, G. McNabb, A. McNabb, S.H. Goh, S. Henwick, C. Astell, J.P. Guo, M. Drebot, R. Tellier, F. Plummer, R.C. Brunham
An outbreak of human coronavirus OC43 infection and serological cross-reactivity with SARS coronavirus
Can. J. Infect. Dis. Med. Microbiol., 17 (6) (2006), pp. 330-336, 10.1155/2006/152612
CrossRef View Record in Scopus Google Scholar

[47] A.C.R. Hoste, A. Venteo, A. Fresco-Taboada, I. Tapia, A. Monedero, L. López, M.F. Jebbink, E. Pérez-Ramírez, M.A. Jimenez-Clavero, M. Almonacid, P. Muñoz, J. Guinea, C. Vela, L. van der Hoek, P. Rueda, P. Sastre

Two serological approaches for detection of antibodies to SARS-CoV-2 in different scenarios: a screening tool and a point-of-care test

Diagn. Microbiol. Infect. Dis. (2020), p. 115167, 10.1016/j.diagmicrobio.2020.115167
(Epub ahead of print. PMCID: PMC7417941)